

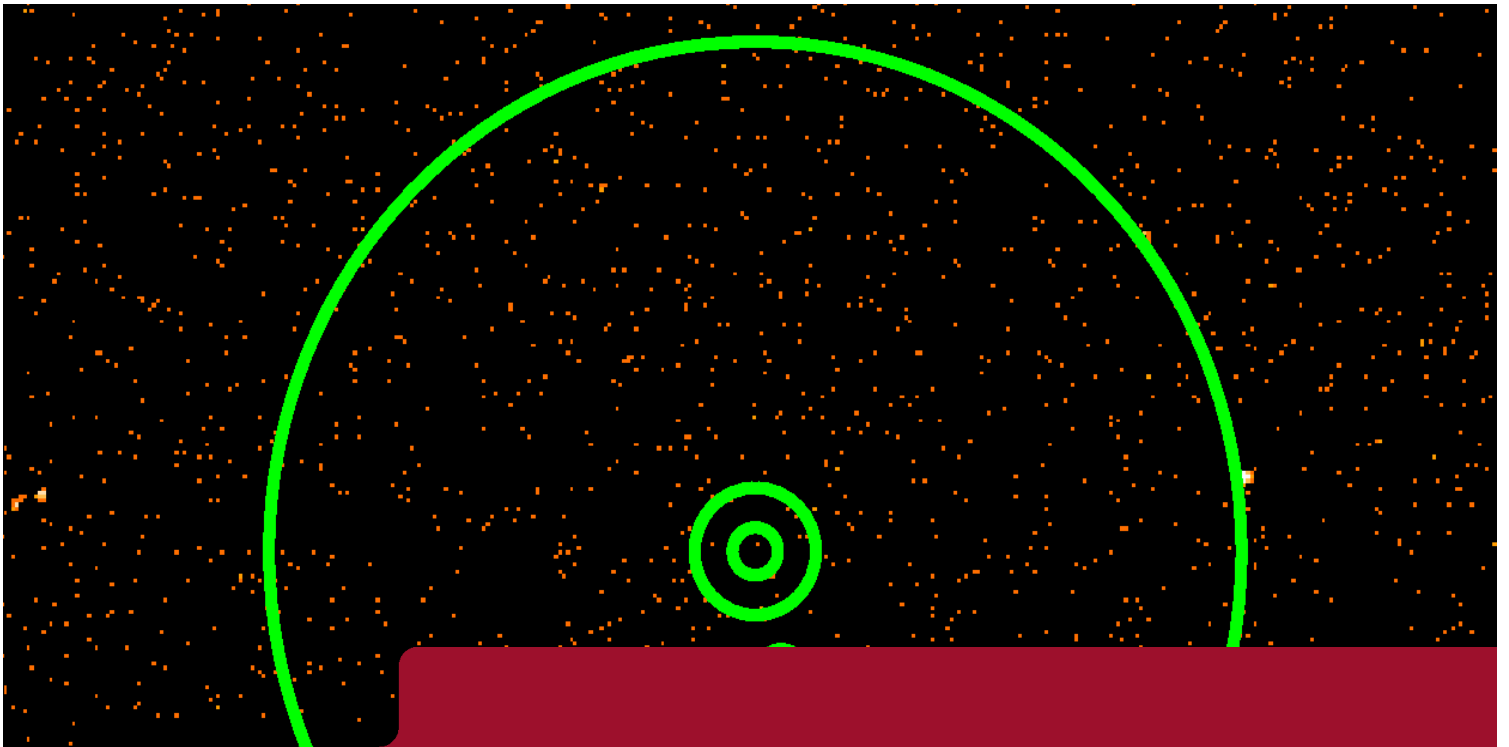


DEGREE PROJECT IN TECHNOLOGY,  
FIRST CYCLE, 15 CREDITS  
*STOCKHOLM, SWEDEN 2021*

# **Investigating the central engine in supernova 2022ap using X-ray observations**

**AMANDA HELMFRID**

**RICHÁRD BAGI**



**KTH ROYAL INSTITUTE OF TECHNOLOGY  
SCHOOL OF ENGINEERING SCIENCES**



Particle and Astroparticle Physics

# Investigating the central engine in supernova 2002ap using X-ray observations

Amanda Helmfrid, Richárd Bagi  
helmfri@kth.se, bagi@kth.se

SA114X Degree Project in Engineering Physics, First Level

Department of Physics

KTH Royal Institute of Technology

Supervisors: Dennis Alp, Josefin Larsson

4th June 2021

## Abstract

Supernovae (SNe) are explosions following the death of massive stars. Core-collapse supernovae (CCSNe) occur when the heavy iron core of these stars collapse in on themselves. The resulting remnant of the core of a CCSN is a compact object: either a black hole or a neutron star. During the collapse and following explosion, massive amounts of energy and material are expelled. The compact objects emit high-energy radiation. With X-ray astronomy, we can observe it and study the processes behind these events. In this thesis, we determine a limit on the X-ray luminosity of SN 2002ap, and constrain the parameters for the magnetic field of the central object, potentially a neutron star. We model the absorption of the radiation by the material in the surrounding area, the so-called SN ejecta, as well as the absorption by the interstellar medium (ISM). We construct the model using the spectral fitting program XSPEC. Assumptions about the abundance of X-ray absorbing elements in the ejecta and ISM are based on earlier models and the explosion energy is taken from previous estimations. The mass of the ejecta is assumed to be  $2.5 - 5 M_{\odot}$  and the distance 9.34 Mpc. We compare the absorption model to the data taken by the Chandra telescope in 2018. From this comparison, we determine the maximum luminosity to be  $L \lesssim 2 \times 10^{40} \text{ erg s}^{-1}$  and constrain the magnetic field to a minimum of  $B \gtrsim 3 \times 10^{13} \text{ G}$ .

## Sammanfattning

När massiva stjärnor dör resulterar de i kraftiga explosioner som kallas supernovor (SNe). En vanlig typ kallas kärnkollapssupernova (CCSN). Denna typ av SN inträffar när stjärnornas tunga järnkärna kollapsar och faller in på sig själv. Resterna av kärnan av CCSNe är kompakta objekt: svarta hål eller neutronstjärnor. Massiva energi- och materialmängder slungas ut under kollapsen och explosionen. De kompakta objekten sänder ut högenergetisk strålning som vi kan observera med hjälp av röntgenteleskop. Observationerna kan vi sedan använda för att undersöka processerna bakom dessa händelser. I den här uppsatsen presenterar vi en luminositetsgräns på SN 2002ap och begränsar den magnetiska fältstyrkan av dess centrala objekt, en potentiell neutronstjärna. Vi modellerar hur mycket strålning som absorberas i dess kringliggande område, i supernovans så kallade ejekta, och även i det interstellära mediet (ISM). Vi ställer upp modellen med spektralanalysprogrammet XSPEC. Antagandena om mängderna av de röntgenstrålningsabsorberande ämnena i ejektat samt i ISM:et grundas på tidigare modeller och explosionsenergin är tagen från tidigare estimeringar. Ejektats massa antas ligga mellan  $2.5 - 5 M_{\odot}$  och avståndet uppskattas till 9.34 Mpc. Vi jämför absorptionsmodellen med datan som hämtades av Chandrateleskopet år 2018. Med denna jämförelse hittar vi den maximala luminositeten  $L \lesssim 2 \times 10^{40} \text{ erg s}^{-1}$  och vi begränsar den magnetiska fältstyrkan till ett minimum  $B \gtrsim 3 \times 10^{13} \text{ G}$ .

# Contents

<b>Abstract and Sammanfattning</b>	<b>2</b>
<b>1 Introduction</b>	<b>5</b>
<b>2 Theoretical background</b>	<b>7</b>
2.1 X-ray astronomy . . . . .	7
2.2 X-ray telescopes . . . . .	7
2.2.1 The Chandra telescope . . . . .	8
2.3 Supernovae . . . . .	9
2.3.1 Supernova classifications . . . . .	10
2.3.2 Core collapse . . . . .	10
2.3.3 Neutron stars . . . . .	11
2.3.4 Magnetars and pulsars . . . . .	12
2.3.5 Luminosity of a neutron star . . . . .	12
2.4 Absorption processes . . . . .	14
2.4.1 Absorption in the ejecta . . . . .	15
2.4.2 Absorption in the ISM . . . . .	17
2.5 Redshift . . . . .	17
<b>3 Investigation</b>	<b>18</b>
3.1 Problem . . . . .	18
3.2 Model . . . . .	18
3.2.1 Absorption model in XSPEC . . . . .	19
3.2.2 Explosion energy and time . . . . .	22
3.3 Analytical calculations . . . . .	22
3.4 Bolometric luminosity of SN 2002ap . . . . .	24
3.5 Results . . . . .	25
3.5.1 X-ray absorption . . . . .	25
3.5.2 Constraining luminosity parameters . . . . .	26
3.5.3 Compiling results . . . . .	29

<b>4</b>	<b>Discussion</b>	<b>30</b>
4.1	Initial rotation period . . . . .	30
4.2	Limitations and future observations . . . . .	32
<b>5</b>	<b>Summary and conclusions</b>	<b>34</b>
	<b>Bibliography</b>	<b>35</b>

# Chapter 1

## Introduction

Supernovae (SNe) are luminous stellar explosions following the death of massive stars. Supernovae are some of the most violent astronomical events known and are responsible for the birth of black holes and neutron stars. Their luminosity is comparable to their host galaxies and can be visible with bare eyes on the night sky. Chinese astronomers found a supernova as early as 185 AD, and called it a “guest star”. Its remnant is still visible today, almost 2000 years later.

Nowadays, astronomers find hundreds of supernovae each year. We have more newly discovered supernovae to be studied than we have time and ways to analyse them. There is yet a lot to learn about supernovae and how they develop throughout their life cycles. Therefore, another important aspect of research is to do follow-up studies with new spectral analysis methods. Here, we will revisit a supernova discovered nearly 20 years ago.

When massive stars collapse they expel large amounts of materials, corresponding to several solar masses ( $M_{\odot}$ ), into its surroundings. This process produces new, heavier elements, contributing to the chemical evolution of the universe. Many of these elements are essential building blocks in planetary formation. For example, elements such as iron makes up a substantial part of our Earth. Even our bodies contain material originating from the supernova responsible for our existence. The shock wave from these explosions also aid in the formation of new stars by compressing surrounding gas and dust.

Neutron stars and black holes are the central compact objects formed as a result of supernovae. Both of them are extreme astronomical objects. The difference in outcome can often be credited to the mass of the progenitor stars. Neutron stars have short rotational periods and small, dense cores. They act as engines for the ongoing explosion and the result is a highly luminous event.

Traditionally, astronomers have relied on optical observations, studying the visible light spectrum. In the past century, technology has developed and we can examine other parts of the electromagnetic spectrum as well.

In this paper we study the X-ray spectrum of the supernova SN 2002ap in the galaxy M74. We wish to analyse its features to learn more about the luminosity, rotational period and magnetic field of the compact object in the centre. The data we use was collected by the Chandra telescope from NASA, 16 years after the explosion. Shortly after the discovery of SN 2002ap, astronomers concluded that it was more luminous than common supernovae. Previous studies have hypothesised the compact object in SN 2002ap to be a neutron star with a strong magnetic field. These kind of neutron stars are often referred to as magnetars. We aim to constrain the luminosity of the magnetar in the centre of SN 2002ap and compare it with results from research of other, similar objects. To achieve this we configure a model for how much of the X-ray radiation has been absorbed by the supernova ejecta and the interstellar medium.

The theoretical background is presented in Chapter 2. In Chapter 3 we describe the method and choice of parameters for our data-analysis, as well as the results of our models. Chapter 4 contains a discussion and analysis of the results and suggestions for further research. Finally, in Chapter 5 we present a summary and the conclusions of our study.

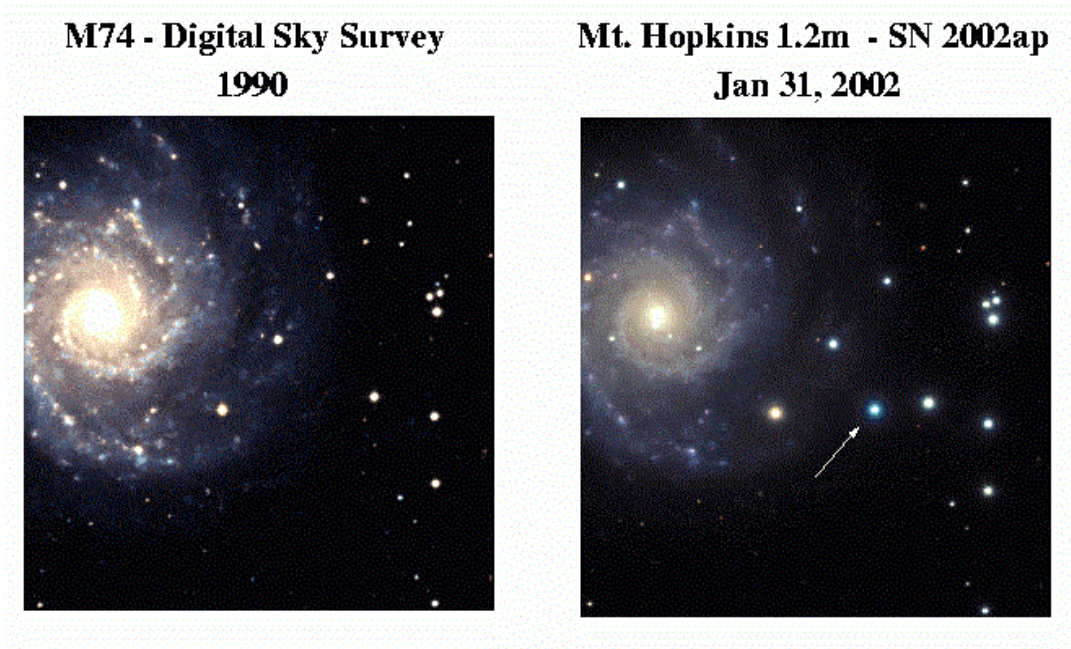


**Figure 1.1:** Image of M74 before and after the explosion. The location of SN 2002ap is indicated by the arrow in the right panel. Credit: Harvard-Smithsonian Center for Astrophysics (2002).

# Chapter 2

## Theoretical background

### 2.1 X-ray astronomy

X-ray astronomy is a field of research aiming to study sources of astronomical X-ray radiation. X-rays have shorter wavelengths and more energy than optical, visible light. Because of this, the X-rays penetrate further into more dense areas. In turn, this makes it possible for astronomers to observe deeper inside extreme astronomical phenomena. This has led to new insights on these events and expanded our understanding of our universe. Some of the greatest sources of X-ray radiation are supernova remnants and neutron stars, which we will study in this thesis.

### 2.2 X-ray telescopes

In the 1990's, astrophysicists launched several new X-ray telescopes. This meant that they could study different areas from an entirely new point of view. With these telescopes, scientists hope to find answers to questions such as how dark matter differs from ordinary matter, or study how supernovae evolve.

X-ray telescopes differ from optical telescopes. In the latter, we use parabolic mirrors, whose axis of symmetry is parallel to the incoming beams of visible light. Then, the mirrors focus the beams into the focal point, where sensors register the incoming photons. In contrast, X-ray telescopes such as Chandra, contain parabolic and hyperbolic mirrors that are almost parallel to the incoming X-ray beams. This is because the X-ray beams are high-energy photons, which are more likely to penetrate the mirrors instead of drastically changing their direction. Therefore, the nearly parallel mirrors will instead reflect the incoming photons with shallow angles into the focal point as shown in Figure 2.1. The surface of these mirrors is so smooth that irregularities are small enough to be at the scale of a few atoms (Harvard-Smithsonian Center for Astrophysics 2013).

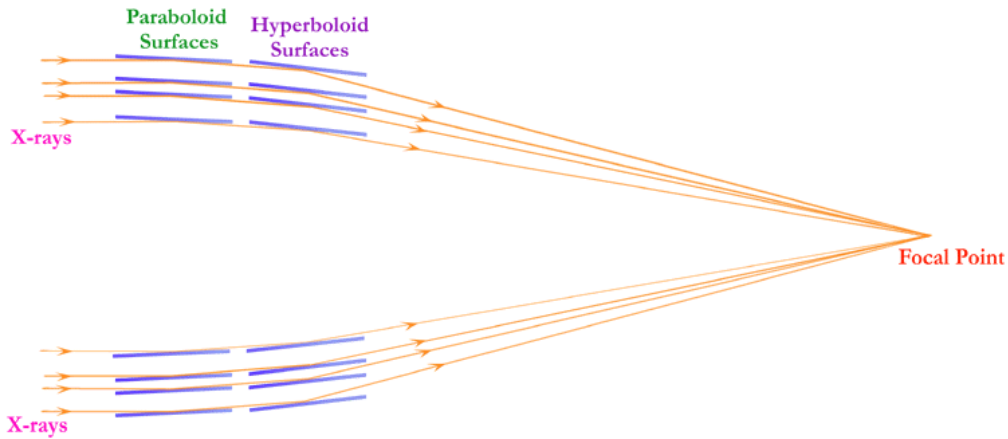


**Figure 2.1:** Illustration of the mirrors of an X-ray telescope. Credit: NASA/CXC/S. LEE (2009).

In the focal point, there are sensors detecting both the position and the energy of the incoming X-rays. This type of telescope is called Wolter telescope (Smale 2018).

A critical difference between optical telescopes and X-ray telescopes are their locations. Optical ones can be stationed on the Earth surface, but X-ray telescopes are required to orbit Earth to be able to observe and collect data. Otherwise, the oxygen and nitrogen in the atmosphere absorb the radiation before it can be detected.

### 2.2.1 The Chandra telescope

In this thesis, we analyse X-ray radiation coming from an astronomical object. To do so, we use data from the Chandra telescope, run by NASA (Harvard-Smithsonian Center for Astrophysics 2014). The most important structural units of this X-ray telescope are the telescope system, composed of four pairs of mirrors, and the unit of scientific instruments collecting data. These include the High Resolution Camera (HRC) and the Advanced CCD (charge-coupled device) Imaging Spectrometer (ACIS), that register sharp images at the focal point of the telescope mirrors. Furthermore, two high-resolution spectrometers are also included, the High Energy Transmission Grating (HETG) and the Low Energy Transmission Grating (LETG), collecting both low and high energy (soft and hard) X-rays (Harvard-Smithsonian Center for Astrophysics 2012). Figure 2.2 showcases the structure of the telescope.

The sensors in the telescope are similar to the ones in optical telescopes, with the difference that the sensors in Chandra are customised for shorter wavelengths. The CCD, containing an array of linked capacitors, converts the X-ray photons to electrons,

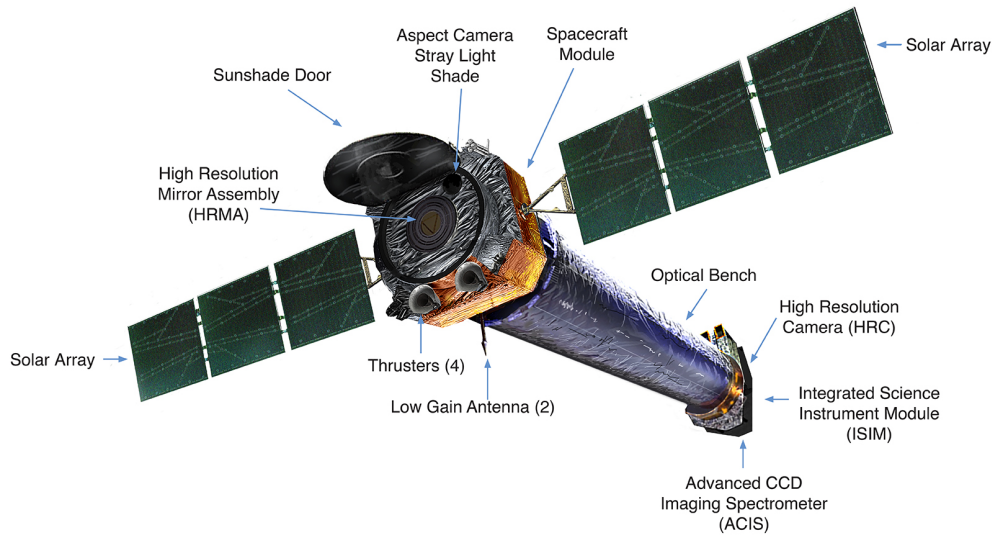


**Figure 2.2:** Illustration of the Chandra-telescope and its components. Credit: NASA/CXC 2019

based on the photoelectric effect. The electrons are then passed on for signal processing (Hondongwa and Fossum 2014).

## 2.3 Supernovae

A central subject of research within X-ray astronomy is supernovae (SNe) and SNe remnants, since they are some of the brightest known X-ray sources. A supernova is a luminous stellar explosion, indicating the death of a massive star (Janka et al. 2007). Most often the explosion is initiated by a collapse in the core of the star (usually consisting of iron). This type of supernova is called a core-collapse supernova (CCSN).

SNe contribute to several important astronomical processes. One example is the life-cycles of stars and planets, since the heavier elements ejected in the explosion change the chemical composition of solar systems and the interstellar medium. The powerful shock waves also compress gases and dust in the remnants' vicinity. On Earth, the oxygen, carbon and silicon, present in rocks ( $\text{SiO}_2$ ), water ( $\text{H}_2\text{O}$ ) and organic molecules, all originate from old SNe.

### 2.3.1 Supernova classifications

SNe are classified according to properties such as presence of certain elements and light curves. Currently, we distinguish two main types of SNe, namely Type I and Type II. The difference between the two types is that Type I SNe lack hydrogen emission lines, implying a hydrogen-poor environment, while Type II SNe do show such lines in the spectrum, indicating a hydrogen-rich environment (Nicholl et al. 2017). In addition, abundance of other elements leads to more sub-classes of Type I and Type II. Previous assessments of the SN studied in this thesis (SN 2002ap) have classified it as a Ic-BL SN (Wang et al. 2017). The Type Ic means that it is not only lacking hydrogen, but also helium. The BL stands for broad lined and refers to them having broad spectral features, as a result of higher kinetic energies (Taddia et al. 2019).

Stellar explosions that are significantly more luminous than usual SNe are called superluminous supernovae (SLSNe). SLSNe emit about 100 times greater amount of energy than usual SNe. SLSNe are also divided into Type I and Type II, on the same principles as ordinary SNe. Both Type I SLSNe and Ic-BL SNe are believed to have higher levels of energy since they share a similar kind of central engine, which powers the explosion.

### 2.3.2 Core collapse

Approximately two thirds of all observed SNe, including the one we study in this thesis, are CCSNe. This type of SN usually results in either a neutron star or a black hole, depending on the mass of the dying massive star.

In the centre of massive stars, an iron core is formed due to fusion. As its mass and volume increase, the electrons in the core are pressed together by the gravitational effect of the star's different layers. However, being fermions, they are governed by Pauli's principle and may not occupy the same quantum state: they show a quantum degeneracy pressure against the increasing gravity.

Since only fusion of nuclei with masses up to iron produces energy, heavier elements cannot be produced in stellar cores. However, after a while the star runs out of fuel, and the iron core reaches a critical mass. At this point, the gravity pressure overcomes the electron degeneracy pressure. Hence, the gravity causes the core to collapse in on itself (Janka et al. 2007). During the collapse, the electrons are pressed into the iron nuclei. Now, a chain reaction of electron capture starts in the stellar core, where protons are transformed to neutrons according to the relation

$$e^{-} + p^{+} = n^{0} + \nu_{e}. \quad (2.1)$$

This results in a large number of emitted electron neutrinos. As the number of electrons decreases, the degeneracy pressure decreases as well, which accelerates the collapse.

Once the collapse has been initiated, the inner parts of the star will continue to collapse into either a neutron star or a black hole. As the electron capture chain reaction goes on, the density of the stellar core increases. When the core reaches the density comparable to that of atomic nuclei, the neutrinos are trapped in the core. The neutrons, also being fermions, exert a the same kind of degeneracy pressure against the increasing gravity pressure as the electrons did in earlier phases. If this degeneracy pressure is also overcome by the gravity, the collapse will result in a black hole. If not, the neutrinos escape the core. A fraction of them heat up the core, and a star explosion is initiated (Janka et al. 2007). Then, the core turns into a neutron star.

### 2.3.3 Neutron stars

Neutron stars get their name from the characteristic neutron composition of their cores. These are the neutrons that were fused from protons and electrons under the immense forces taking place during the collapse. As the progenitor star collapses, the radius of its core decreases from an order of  $10^5$  km to approximately 10 km, while also maintaining the same angular momentum. This results in the neutron stars gaining rotational periods of only a few milliseconds.

In order to understand neutron stars better, we need to examine their formation in further detail. During the core collapse, as mentioned, many neutrinos are emitted. If the kinetic energy from 1 % of them is absorbed, it will power the SN explosion (Janka et al. 2007). The required explosion energy depends on the gravitational binding energy. The absorbed kinetic energy must counteract the gravity in order to minimise the amount of material falling back on the core. This way, the mass increase of the core is kept low, letting the neutron degeneracy pressure counteract smaller gravity pressure. If the core mass is kept below  $2 M_{\odot}$ , a neutron star is formed at the centre, otherwise a black hole is formed.

The neutron degeneracy pressure halts the collapse and heats up the core to  $10^{10}$  K (Janka et al. 2007). At this temperature, the core emits neutrino-antineutrino pairs of all flavours, as well as high-energy photons, by thermal emission. The total number of emitted neutrinos is several orders of magnitude greater than during the previous, electron capture phase. Due to the stalled collapse, a characteristic bounce shock wave propagates out from the core out to the outer layers of the exploding star. Consequently, this makes it possible for the outer shells to bounce off the core and have time to absorb 1 % of the kinetic energy of the neutrinos. This neutrino absorption heats up and changes the chemical composition of the surrounding material, resulting in a thermal expansion of the innermost layers. New and heavier elements are then produced as the temperature rises.

Because of the collapse and subsequent explosion, most of the star's matter has been dispersed around it and we call this the SN ejecta. Observations have shown that the

ejecta are not evenly distributed (Alp et al. 2018). Exactly how and why this occurs is still a matter of active research. However, in our model, we assume that the ejecta are spherically symmetric for simplicity, since we lack information about the exact ejecta distribution in the studied SN.

### 2.3.4 Magnetars and pulsars

To understand why these explosions release such high amounts of energy, we study one of the existing current models, the magnetar model (Nicholl et al. 2017). In this model, the energy source is a neutron star with an extremely strong magnetic field, called a magnetar. This is a newly-formed neutron star created by the core collapse, having high frequency rotation,  $P \approx 1 - 8$  ms. A neutron star that has a strong magnetic field of  $B \approx 10^{14}$  G<sup>1</sup> loses large amounts of energy due to the rapid rotation (Nicholl et al. 2017). This way, the energy emitted by the neutron star can reach the high levels of explosion energy of SN Type Ic-BL and SLSN Type I discussed in section 2.3.1.

Pulsars are pulsating neutron stars. They emit beams of radiation, possibly along the magnetic axis, and when these coincide with our line of sight we see short bursts of the radiation (Karttunen et al. 2007). The short rotational periods and strong magnetic fields, combined with this pulsating effect, create a flickering which we cannot see without the help of powerful telescopes.

Neutron stars can be classified as being magnetars, pulsars or a combination of both. However, the terminology is not always consistent and sometimes depend on context. Section 2.3.5 goes more in depth into the relationship between the magnetic field, rotational period and luminosity.

### 2.3.5 Luminosity of a neutron star

Luminosity is a measure on how much electromagnetic radiation an object emits during a time unit. Since the examined object is in another galaxy, we can only study the light coming from the source. Therefore, it is important to understand how the luminosity of the object behaves. This way, we can understand the processes leading the time development of the observed phenomena.

When modelling a neutron star, we can approximate the system as a rotating magnetic dipole. The main properties of this system are thus the magnetic field  $B$  of the dipole and the rotational period  $P$  of the neutron star. After the core collapse, the central object of the supernova contracts to a radius of  $R \approx 10$  km. As a consequence, the rotation period gets significantly smaller, resulting in a high frequency spin, due to preservation of angular momentum and the drastically decreased spatial dimensions. The magnetic field

---

<sup>1</sup>In astronomy, one uses the unit G instead of T ( $1 \text{ G} = 10^{-4} \text{ T}$ ) to denote magnetic field strengths by convention.

of the remaining object, the neutron star, remains at the same high level of around  $10^9$ – $10^{15}$  G (Manchester et al. 2005). We shall note that the rotation axis and the magnetic axis need not coincide. The angle  $\alpha$  between them also influences the energy loss with a factor  $\sin^2 \alpha$  (Condon and Ransom 2016). For simplicity, we assume that the axes are perpendicular to each other, that is,  $\alpha = \pi/2$ , corresponding to a maximal energy loss. The star loses energy due to the fact that the spinning magnetic field generates electromagnetic waves. This results in an increase in the rotational period. Therefore, we call the luminosity of the neutron star spin-down luminosity. We identify the neutron star's total energy decrease with this luminosity. Additionally, we note that the slower rotation results in the luminosity decreasing over time. Assuming the neutron star to be spherically symmetric and homogeneous, the radiated energy per unit time is then described by

$$\dot{E} = -\frac{4\pi^2 I \dot{P}}{P^3} = -\frac{2^5 \pi^4 R^6 B^2}{3c^3 P^4}, \quad (2.2)$$

where  $I$  is the moment of inertia of the neutron star,  $c$  is the speed of light,  $P = P(t)$  is its rotational period,  $\dot{P} = \dot{P}(t)$  is the time derivative of the rotational period,  $R$  is the radius and  $B$  is the magnetic field strength.

Furthermore, under the assumption that this radiated energy equals to the spin-down luminosity,  $L = -\dot{E}$ , we find the relation between the magnetic field strength  $B$ , the period time  $P$  and the luminosity  $L$  to be

$$L = \frac{2^5 \pi^4 R^6 B^2}{3c^3 P^4}. \quad (2.3)$$

Then, since the rotation period is not stationary, we take the characteristic age  $\tau = P/2\dot{P}$  of the neutron star into account (Condon and Ransom 2016). Now, we find the luminosity as a function of the initial period  $P_0$ :

$$L = \frac{2^5 \pi^4 R^6 B^2}{3c^3 P_0^4 (1 + t/\tau)^2}, \quad (2.4)$$

where  $t$  is the elapsed time after the core collapse. Now, combining the previous three equations, we find the initial period as a function of the period at a given time  $t$  after the explosion:

$$P_0 = \sqrt[4]{\frac{9c^6 P^8(t)}{(3c^3 P^2(t) + 2^4 \pi^2 R^6 B^2 t)^2}}. \quad (2.5)$$

However, we can only measure a fraction of this luminosity since it is radiated spherically symmetrically outwards from the neutron star. This fraction is called the flux, the

proportion of the luminosity traversing a unit area of the sphere of a radius  $D$  around the neutron star. Thus, the flux  $F$  is given by the relation

$$F = \frac{L}{4\pi D^2}, \quad (2.6)$$

where  $D$  is the distance between the pulsar and us.

One thing we need to take into consideration is that the flux we measure only represents a part of the whole spectrum, since telescopes measure radiation within a limited energy interval. For example, in this study, we will attain a luminosity corresponding to the X-ray energy interval of 2 – 10 keV. Therefore, we need to find a proportion between the luminosity of the limited energy interval and the total luminosity, the so called bolometric luminosity. For young pulsars, the reference value is the one identified at the Crab nebula, where 1.6 % of the emitted energy corresponds to the 2 – 10 keV X-ray radiation interval. Assuming this relation to be general, we find

$$L_{2-10\text{keV}} = 0.016L, \quad (2.7)$$

where  $L_{2-10\text{keV}}$  can be found using equation (2.6) and  $L$  is the bolometric luminosity.

## 2.4 Absorption processes

When observing celestial bodies we often lack the possibility to travel to the objects and make measurements in proximity to them. Thus, we must observe the particles coming from the objects, which are mainly photons. Photons interact easily with the matter that lies between the source and the observatory. For this reason, all radiation emitted by the source along our line of sight does not necessarily reach us. To be able to study the radiation that reaches our telescopes, we have to think about what has happened to the radiation on the way and set up a model that takes absorption into account. Since the X-rays do interact with matter of different kinds we have to make an absorption model that takes both the abundances and the chemical properties of these elements into consideration.

Regarding a magnetar in the centre of a new SN, there are three main regions between the source and the telescope that contain material: the SN ejecta, the host galaxy and the Milky Way. The two latter are referred to as the interstellar medium (ISM). However, since most of the material on the accounted line segment is situated in the ejecta, most of the absorption takes place there.

Having X-ray photons interacting with matter, there arises two main types of absorption. One of them is Compton scattering, which happens when a photon scatters off an electron. The electron then gets kinetic energy, supplied by the incoming photon. However, only a fraction of the photon's energy is converted into kinetic energy. Thus,

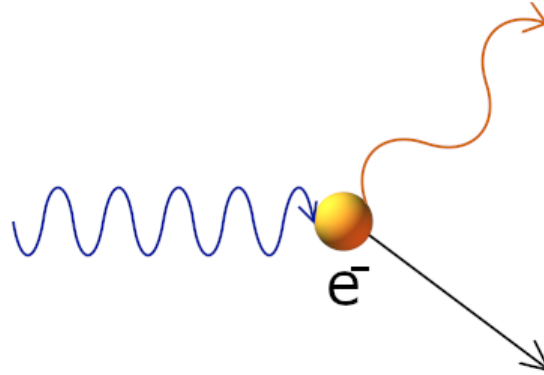


**Figure 2.3:** Illustration of Compton scattering off a free electron.

the photon travelling further has a lower energy, as shown in Figure 2.3. Then, the momentum conservation determines the orientation of the photon's and the electron's new path.

The other absorption process is the photoelectric absorption. In this process a bound electron absorbs a photon, using all its energy to excite to a higher energy level, or, to decouple from the atom and ionise it (Berkowitz 1979), as shown in Figure 2.4. Hence, this requires that the material is not fully ionised. In contrast to Compton scattering, where the photon is scattered with a new, longer wavelength, photoelectric absorption destroys the photon involved in the process.

### 2.4.1 Absorption in the ejecta

Right after the explosion, the ejected material consists mostly of ions and all electrons are free in the plasma. The only X-ray-material interaction taking place at this time is Compton scattering. This transforms the X-rays to lower energy photons, making the SN impossible to observe in this energy region. This is why SNe are usually discovered as they appear on the night sky visible in the optical spectrum.

With time, the expanding ejecta cools down and the ions bind free electrons. The bound electrons result in photoelectric absorption as well, mainly in the region between 2 – 10 keV. Thus, the photons are now hindered from escaping due to the large amounts

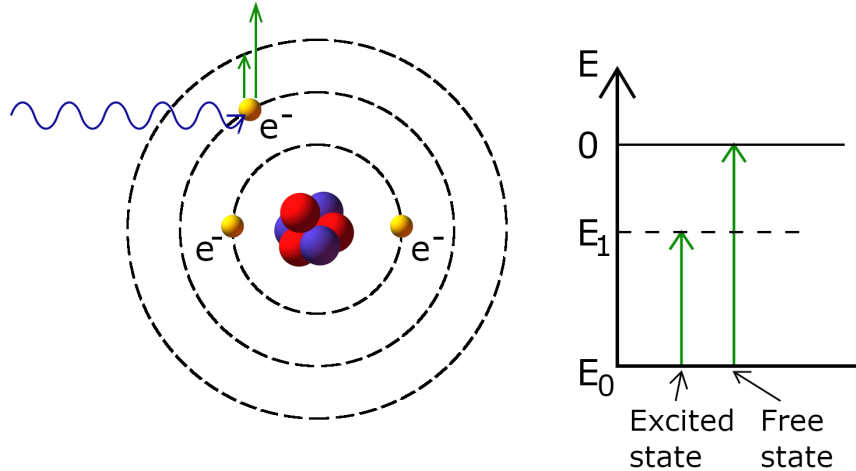


**Figure 2.4:** Illustration of photoelectric absorption. Corresponding energy levels are depicted on the right hand side.

of atomic particles in the ejecta. Atoms make the ejecta optically thick<sup>2</sup> in the X-ray region and they block the path from these photons (Metzger et al. 2014). Hence, no X-rays in the energy interval 2 – 10 keV can leave the system during the first months.

However, on longer timescales, we find that X-rays do succeed in escaping the ejecta. One possible process where the X-rays get through the SN ejecta according to the magnetar model is ionisation break-out (Metzger et al. 2014), where all the atoms in the ejecta get ionised by absorbing the incoming X-rays from the magnetar. Once the entire cloud of ejecta is ionised the X-rays may escape without getting absorbed completely.

Another possible process is that the expanding material simply dissipates enough for the photons to get through after some years. Until then, the main absorption process is the photoelectric absorption. We note that since the bound electrons have distinct binding energies, they mostly absorb photons with lower energies (in the soft X-ray interval), instead of absorbing higher energy photons (hard X-rays and  $\gamma$ -photons). Both of these models explain why we only can detect X-rays in the mentioned energy interval after some years following the explosion.

<sup>2</sup>The depth that radiation can reach in a material depends on the photon energies. In other words, the absorption is wavelength dependent within a medium. Practically, if absorption is high in an interval of wavelengths, the medium is optically thick in this region, and optically thin for other intervals.

### 2.4.2 Absorption in the ISM

We can now move on to the absorption in the interstellar medium. In the ISM there are mainly atoms and molecules with small atomic numbers. These can be surveyed, which has been done by Wilms et al. (2000). In the model described in Chapter 3, we use the term column number density. This term stands for the number of particles of a specific material along the line of sight between the object and the observer over a unit area. It is often given in the form  $\text{cm}^{-2}$ , expressed as column density. Normally the particles in the ISM are, as mentioned above, atoms or molecules where bound electrons can become excited. Thus, photoelectric absorption is the main absorption form in the ISM. Due to the photoelectric absorption in the ISM, the cross section<sup>3</sup> is a quickly decreasing function of the photon energy. Furthermore, the opacity of each wavelength is proportional to the number of particles that are able to absorb the incoming photons, which makes column number density a good measure of the interstellar absorption.

## 2.5 Redshift

In astronomy it is common to use redshift as a measure of distance. When a wave source is moving relatively to an observer, such as an ambulance car relatively to a pedestrian, the observer may detect the wave of a different frequency than the frequency in the source's reference system. The frequency change depends on the velocity difference. This effect is called the Doppler effect. On longer length scales, the same effect can be seen as a shift in the frequency of the light. The light of a source, moving fast away from the observer, is shifted towards lower frequencies. In the optical region, this means that the light seems to be redder. Therefore, the Doppler effect for light is called redshift.

As the universe is expanding, matter will spread out. Thus, from our perspective on Earth, galaxies are moving away from us. If a light source is moving with velocity  $v$ , then the redshift can be described with  $z = v/c$ . Hubble has found a linear relation between this redshift and the distance  $d$  of celestial objects (Gelderman 2012):

$$d = \frac{c}{H_0} z, \quad (2.8)$$

where  $H_0$  is the Hubble constant. Thus, we can use the redshift of an astronomical object to determine its distance.

---

<sup>3</sup>The cross section denotes the probability of a given interaction between two particles (Fermilab 2013).

# Chapter 3

## Investigation

### 3.1 Problem

The supernova we study in this thesis is SN 2002ap, which is thought to host a magnetar in the centre. The aim of this project is to constrain the properties of this magnetar, with the intention of finding the maximum allowed X-ray luminosity. Furthermore, we relate the luminosity to its magnetic field strength and rotation period.

When SN 2002ap was observed for the first time it gained attention for its high luminosity and relative proximity to Earth. Amateur astronomer Yoji Hirose discovered it on 18th January 2002 at the celestial coordinates  $[01^{\circ} 36' 23.90''; +15^{\circ} 45' 13.2'']$ , at a distance of 9.34 Mpc. Early studies mostly analysed the UVOIR<sup>1</sup> spectrum of SN 2002ap, whereas we use X-ray observations of it, taken 16 years after the explosion. The measurements used in this project were taken by the Chandra X-ray telescope on the 4th of November 2018 with an exposure time of 16050 s.

### 3.2 Model

Aiming to study the luminosity of SN 2002ap, we go through a few steps to model how emission from the centre of the SN would be affected by absorption, based on the data from Chandra. The idea is to develop a model for how much of the radiation that has been absorbed by the ejecta and ISM. This means that we have to make assumptions about the abundances of elements, based on other SN simulations.

In this study we use XSPEC to analyse the X-ray spectra from SN 2002ap. XSPEC is an X-ray spectral-fitting program developed and maintained by NASA. It can be used to analyse data from several telescopes and observatories (Arnaud et al. 2020). Using the different modelling tools in XSPEC, we get a model of the expected rate of photons we

---

<sup>1</sup>Ultraviolet (UV), optical (O) and infrared (IR) region of the spectrum.

would be able to observe if there was no absorption for a given luminosity. Furthermore, with the data from Chandra we calculate a statistical limit  $k$  on the expected number of photons coming from the source. This limit implicates that if we expect at most  $k$  photons to pass the observatory under a given time at our distance from the source, then we have a 99.7 % probability to detect only 1 photon. Thus, the X-ray radiation source must be fainter than this limit, see Chapter 3.3 for details. Comparing these different photon limits, the one from the XSPEC model and the one from the data, we can determine the upper limit of the flux of SN 2002ap. With the flux limit we then calculate the maximum allowed luminosity.

X-rays, being ionising high-energy radiation, have photon energies between 0.1 – 100 keV. However, the Chandra telescope can only observe X-ray radiation in the interval from 0.3 – 10 keV. Modelling a fast rotating magnetar, we assume that 1.6 % of the emitted radiation lies in the soft X-ray energy region from 2 – 10 keV, according to equation (2.7). Furthermore, as we will see in the next chapter, the radiation under  $\sim 2$  keV is practically completely absorbed in our model. Therefore, we limit ourselves to the energy interval 2 – 10 keV in our luminosity calculations.

### 3.2.1 Absorption model in XSPEC

As mentioned in section 2.4, we have to take the absorption into account when analysing our data. The model components we use in XSPEC can work in three different ways. The first is additive, where the models represent sources of emission and produces a theoretical spectrum. In this thesis for example, the represented source of emission is the X-ray radiation coming from SN 2002ap. The components can also be multiplicative. This type is meant to use an energy-dependent factor to modify the spectrum produced by additive components. The last type used for our model is convolution, which is able to combine other models by applying a convolution operator.

To model the absorption from the ejecta in XSPEC we combine four pre-programmed components: `tbvarabs`, `tbabs` and `clumin` and an emission power law. We now present the used model components in detail. Further information about them can be found in the XSPEC user’s guide manual (Arnaud et al. 2020). In Table (3.1) we present the final parameters used for the absorption model in XSPEC.

#### `powerlaw`

There needs to be at least one additive model component, since there must be a source of emission. For our absorption model we use the built-in `powerlaw`. This component is a simple photon power law, where the photons are distributed according to

$$A(E) = KE^{-\alpha}, \quad (3.1)$$

where  $K$  is a normalisation constant,  $E$  is the energy and  $\alpha$  is the photon index.

### **tbabs**

The first multiplicative model we need for our absorption model is **tbabs**. With **tbabs** we can include the absorption in the Milky Way. For **tbabs** we simply need the hydrogen column density for the line of sight to SN 2002ap. To find it, we use an online calculator<sup>2</sup> developed by Willingale et al. (2013).

### **tbvarabs**

The second of the two multiplicative components we use is **tbvarabs**. So far we have considered the X-ray absorption processes in the Milky Way and now we focus on the absorption in the SN itself. **tbvarabs** lets the user enter parameter values for the different element abundances in the SN ejecta, since they contribute to the absorption differently depending on the composition of the ejecta. It also takes the redshift into account as another parameter. We base this model on the ISM absorption model presented in J. Wilms et al. (2000). We adjust the parameters to typical SN ejecta data from Table 2 in Alp et al. (2018). This table presents different models, consisting of proportions for abundances for different kinds of SNe, where we use the model B15<sup>3</sup> to model SN 2002ap.

One of the main differences in composition of the ISM and SN ejecta is the higher metallicity of the latter, meaning that there is a large presence of elements heavier than helium. Following this, the model turns a bit problematic, since the absorption is quantified by the hydrogen column density and the standard abundances of other elements are assumed in respect to it. Since the SNe investigated in this study lack H I and He I, we want to exclude these from the model. Setting the hydrogen column density to zero is not an option, since the remaining abundances are provided relative to H. Therefore, we have to scale it down instead. The helium abundance can be set to zero. Once hydrogen and helium are removed, there is not much total mass left in the model. This is because hydrogen and helium make up 96 % of the ejecta mass in the B15 model. This means we also have to scale the mass proportions for the rest of the elements such that the final total mass is correct. For the SN 2002ap, the total ejecta mass is estimated to be in the range of  $2.5 - 5 M_{\odot}$  (Mazzali et al. 2002).

### **clumin**

Finally, we use the model **clumin** to compute the 2–10 keV luminosity for our absorption model. This component combines the previous components, so that the observed flux becomes a model parameter. The flux parameter is rescaled such that the modelled flux corresponds to the observational upper photon rate. Within XSPEC, the `model`

<sup>2</sup>The calculator is found on this address: <https://www.swift.ac.uk/analysis/nhtot/index.php>

<sup>3</sup>B15 is an explosion model of SN 1987A.

`predicted rate` is automatically calculated together with the absorption model after choosing all the parameters. Multiplying our `model predicted rate` with the exposure time for the Chandra observations gives us how many photons that the telescope theoretically should have detected as most. Later on, this number can be used to calculate the total luminosity of SN 2002ap.

The combination of these four components constitute our model for the absorption. Table 3.1 presents the values for each non-zero input used to model the absorption.

**Table 3.1:** XSPEC parameters and their set values for the absorption model for SN 2002ap.

<i>Parameter</i>	<i>Description</i>	<i>Value</i>	<i>Unit</i>
<i>nH</i>	H column density num. for the Milky Way	$4.58 \cdot 10^{-2}$	$10^{22}$ atoms $\text{cm}^{-2}$
<i>nH</i>	H column density num. for SN 2002ap	$2.01 \cdot 10^{-4}$	$10^{22}$ atoms $\text{cm}^{-2}$
<i>C</i>	C abundance (relative to ISM)	$4.89 \cdot 10^4$	... <sup>a</sup>
<i>O</i>	O abundance (relative to ISM)	$3.30 \cdot 10^4$	... <sup>a</sup>
<i>Ne</i>	Ne abundance (relative to ISM)	$3.87 \cdot 10^4$	... <sup>a</sup>
<i>Mg</i>	Mg abundance (relative to ISM)	$1.48 \cdot 10^4$	... <sup>a</sup>
<i>Si</i>	Si abundance (relative to ISM)	$2.37 \cdot 10^5$	... <sup>a</sup>
<i>S</i>	S abundance (relative to ISM)	$4.44 \cdot 10^4$	... <sup>a</sup>
<i>Ar</i>	Ar abundance (relative to ISM)	$8.42 \cdot 10^4$	... <sup>a</sup>
<i>Ca</i>	Ca abundance (relative to ISM)	$6.72 \cdot 10^5$	... <sup>a</sup>
<i>Fe</i>	Fe abundance (relative to ISM)	$1.68 \cdot 10^5$	... <sup>a</sup>
<i>redshift</i>	Redshift from Earth to SN 2002ap	$2.12 \cdot 10^{-3}$	... <sup>a</sup>
<i>Emin</i>	Min. source frame energy <sup>b</sup>	2.00	keV
<i>Emax</i>	Max. source frame energy <sup>b</sup>	10.0	keV
<i>lg10Flux</i>	$\log_{10}$ flux <sup>c</sup>	-13.536	$\text{erg s}^{-1} \text{cm}^{-2}$
<i>PhoIndex</i>	$\alpha$ , photon index of power law	2.00	... <sup>a</sup>
<i>norm</i>	K, normalisation constant	1.00	... <sup>d</sup>

<sup>a</sup> Dimensionless

<sup>b</sup> Over which flux is calculated.

<sup>c</sup> This parameter is rescaled to match `model predicted rate`.

<sup>d</sup> The norm is given in photons  $\text{keV}^{-1} \text{cm}^{-2} \text{s}^{-1}$ , at 1 keV.

### 3.2.2 Explosion energy and time

Another factor to take into consideration is the explosion energy of the model and the actual SN. For SN 2002ap, the ejecta’s kinetic energy is estimated to be  $(4 - 10) \cdot 10^{51}$  erg (Mazzali et al. 2002). Thus the studied supernova expands faster than common SNe with similar ejecta abundances, and we need to rescale the velocities. This affects the column densities, so we need to correct the abundance values accordingly.

We implement the velocity correction by adjusting the development time of the model. We find that the time it would have taken for a similar, reference SN to develop as much as SN 2002ap is proportional to the time elapsed after the SN 2002ap core collapse. The proportionality constant is the quotient of the SN velocities according to the relation

$$t_{\text{ref}} = \frac{v_{02\text{ap}}}{v_{\text{ref}}} t_{02\text{ap}}. \quad (3.2)$$

However, we only have estimations on the total ejecta mass and the total kinetic energy, which only lets us make assumptions on the expansion velocity. For simplicity, we want to only have the mass as variable. As a simple model, we choose to have a linear, one-to-one map from the energy range to the mass range found by Mazzali et al. (2002). They have found that the ejecta mass should be in the range of  $2.5 - 5 M_{\odot}$ , while the kinetic energy range should be between  $(4 - 10) \cdot 10^{51}$  erg. Using the formula for the kinetic energy, we get the velocity

$$v(m) = \left( (\sqrt{1.25} - 1) \frac{m}{m_0} + (2 - \sqrt{1.25}) \right) 1.27 \cdot 10^7 \text{ m/s}, \quad (3.3)$$

where  $m_0 = 2.5 M_{\odot}$ .

Using equations (3.2) and (3.3) we can unambiguously fit the model to arbitrary mass and reduce the number of variables to only one. In our final absorption model, we adopt the ejecta mass  $5 M_{\odot}$ , corresponding to the kinetic energy  $10 \cdot 10^{51}$  erg, following equation (3.3). Nevertheless, this velocity mapping is not general and is only used to simplify the numerical analysis.

By now, we have rescaled the abundances for the model by reducing H, He, increased the other elements to match the estimated mass of SN 2002ap, as well as rescaled the velocity.

## 3.3 Analytical calculations

We calculate a limit for the maximum observed flux consistent with the observation. In our observation, we detected only one photon in the direction of the source. We aim to determine the upper limit of the luminosity of the studied magnetar, for which we

still have the probability 99.7 % of detecting only one photon. We choose to utilise the Poisson distribution in order to find this limit due to the nature of the problem: counting a certain number of photons within a span of time.

In the Poisson distribution formula, the probability  $p$  of getting  $k$  events with a mean value of occurrences  $\lambda$ , is given by:

$$p(\lambda, k) = e^{-\lambda} \frac{\lambda^k}{k!}. \quad (3.4)$$

For a chosen probability, we can solve this equation for  $k$ . This parameter  $k$  corresponds to the expected total number of photons arriving at the telescope during the measurement. In our case, the average value  $\lambda$  is the average number of detected photons in the surrounding region.

Using ds9 (image display and visualisation tool for astronomical data) we are able to load regions for our source and background, as shown in Figure 3.1. With the analysis tool in ds9 we can both examine the background and the source region. Sampling from the background, we find the typical spatial average photon count 0.021 photons pixels<sup>-1</sup>, spread across 112 pixels. This photon count is a sum over the total observation time. This average results in the expectation value  $\lambda = 0.021 \cdot 112 = 2.355$  photons. Using  $\lambda$  and the 99.7 % probability we receive a source flux limit of  $k = 7$  photons. This upper limit on the source luminosity can be used for a comparison in our model made with XSPEC in section 3.2.1.

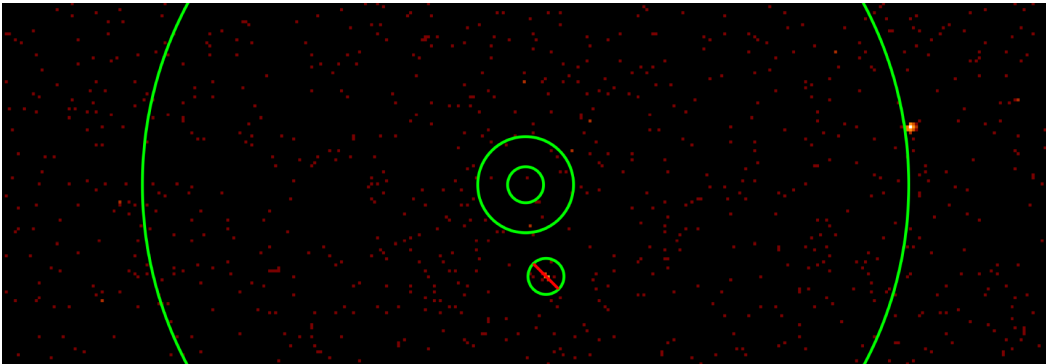


**Figure 3.1:** The source region as observed by the Chandra telescope in 2018. The circle in the centre surrounds SN 2002ap, while the outer circles show the background annulus. The crossed-out small circle in the annulus contains another source, and it is therefore excluded from the background region.

### 3.4 Bolometric luminosity of SN 2002ap

Finally, we compute the maximum allowed total luminosity of SN 2002ap. We combine our XSPEC absorption model and the analytically calculated photon limit from section 3.3 to calculate what source luminosity would yield 7 photons. This is where the flux parameter in our absorption model is critical and it has been rescaled such that the model and observations match. Using equation (2.6) we calculate the 2 – 10 keV luminosity.

The final step is to generalise the luminosity for the entire electromagnetic spectrum. The calculated luminosity is an estimation of the fraction lying in the interval 2 – 10 keV of the total luminosity. To find the bolometric luminosity we use equation (2.7).

We make plots of the luminosity with respect to magnetic field and rotational period, as described by equations (2.3) and (2.4). With these plots we can analyse possible parameters and compare with measurements of other SNe.

## 3.5 Results

### 3.5.1 X-ray absorption

First, we model the absorption in order to find the bolometric luminosity, and then we move on to modelling the strength of the magnetic field of the neutron star.

When modelling, we make the following assumptions: in the centre of SN 2002ap, there is a neutron star, which can be described by the magnetar model (Nicholl et al. 2017). In the SN ejecta, we assume H and He to be lacking (that is, SN 2002ap is of Type Ic-BL), and use the ejecta mass and kinetic energy listed by Mazzali et al. (2002). Furthermore, we assume ordinary ISM and Milky Way absorption. Using these assumptions and abundance values described in Chapter 3.2.1, we get the modelled spectrum, produced by the program XSPEC, presented in Figure 3.2.

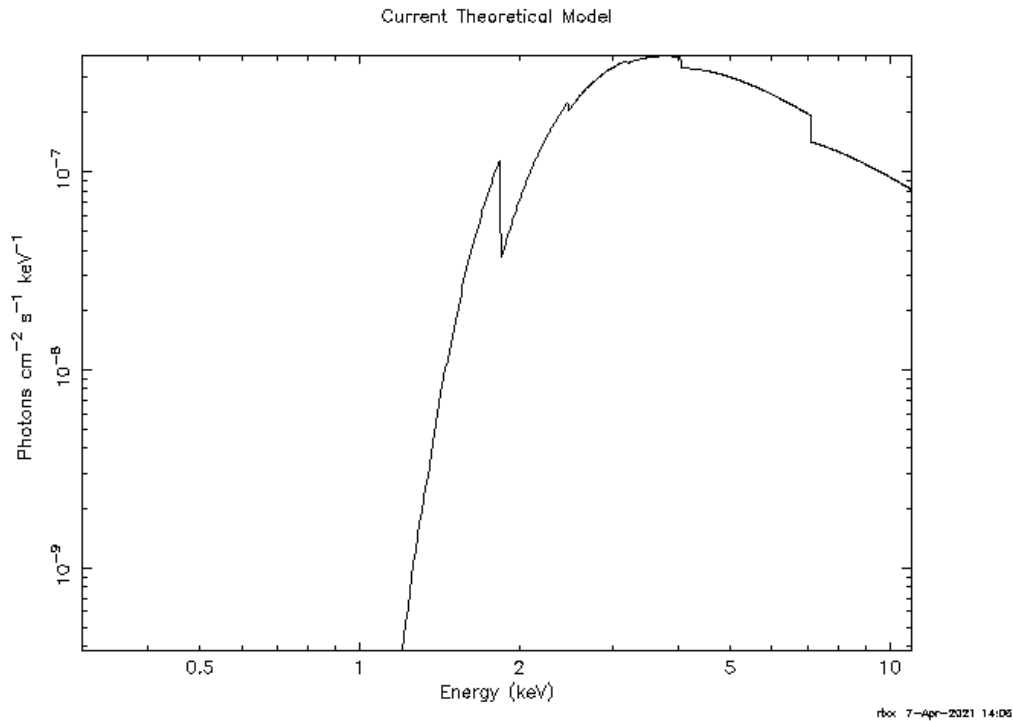


**Figure 3.2:** Absorption model from XSPEC, showing the expected X-ray spectrum from the neutron star in SN 2002ap after absorption in the ejecta and the interstellar medium.

On the vertical axis, we see the flux as the number of photons of given energy observed over unit area, unit time and energy interval. On the horizontal axis, we find the relevant energy range, since the observed X-ray radiation lies within the interval 2 – 10 keV. Integrating over the energy, we get the total number of photons over unit area at our distance from the object in this interval. We combine this photon number, the model predicted rate, with the exposure time of 16 ks, to obtain the total number of photons that we expect to observe. Then, we fit the source flux  $F$  to make the expected number of photons equal to the observed upper limit of 7 photons. Performing these steps, we find that the source flux in the X-ray region must be lower than  $F < 10^{-13.5}$  erg s $^{-1}$  cm $^{-2}$ . Scaling up this flux to the total sphere area at our distance from the source, we get the X-ray luminosity to be

$$L_{2-10\text{keV}} = 3 \cdot 10^{38} \text{ erg s}^{-1} \quad (3.5)$$

according to equation (2.6). This and equation (2.7) result in the total bolometric luminosity

$$L = 2 \cdot 10^{40} \text{ erg s}^{-1} \quad (3.6)$$

At distinct energies we see drops of varying magnitudes in the curve. These are so called absorption edges that arise due to photoabsorption in specific materials in the region between the source and the telescope.

Furthermore, we see that the model only predicts incoming radiation at the higher energy ranges, over  $\sim 1.1$  keV. This result is consistent with the fact that high energy radiation can penetrate more material and get through thicker layers than low energy photons.

### 3.5.2 Constraining luminosity parameters

In equation (3.6) we have found the upper limit on the luminosity that the neutron star in the centre of SN 2002ap might have had during the observation in 2018. Based on this value, we can plot and constrain the period time and magnetic field strength the magnetar might have had at the point of observation, according to equation (2.3). The plot is shown in Figure 3.3.

In the region to the right, we see old pulsars in the Milky Way (and eventually in its satellite galaxies), listed in the ATNF Pulsar Catalogue (Manchester et al. 2005). Since they are old pulsars, their rotation period change has become low and we can assume that their movement to the right in the  $BP$ -plane is slow. Furthermore, we see that their luminosities lay in the range of approximately  $10^{30} - 10^{35}$  erg s $^{-1}$ .

Meanwhile, the red dots to the left are pulsars, in the centre of SLSNe, in their initial states, as estimated in Table 3 by Nicholl et al. (2017). The fact that they are in their initial states, combined with the fact that the model assumes constant magnetic field

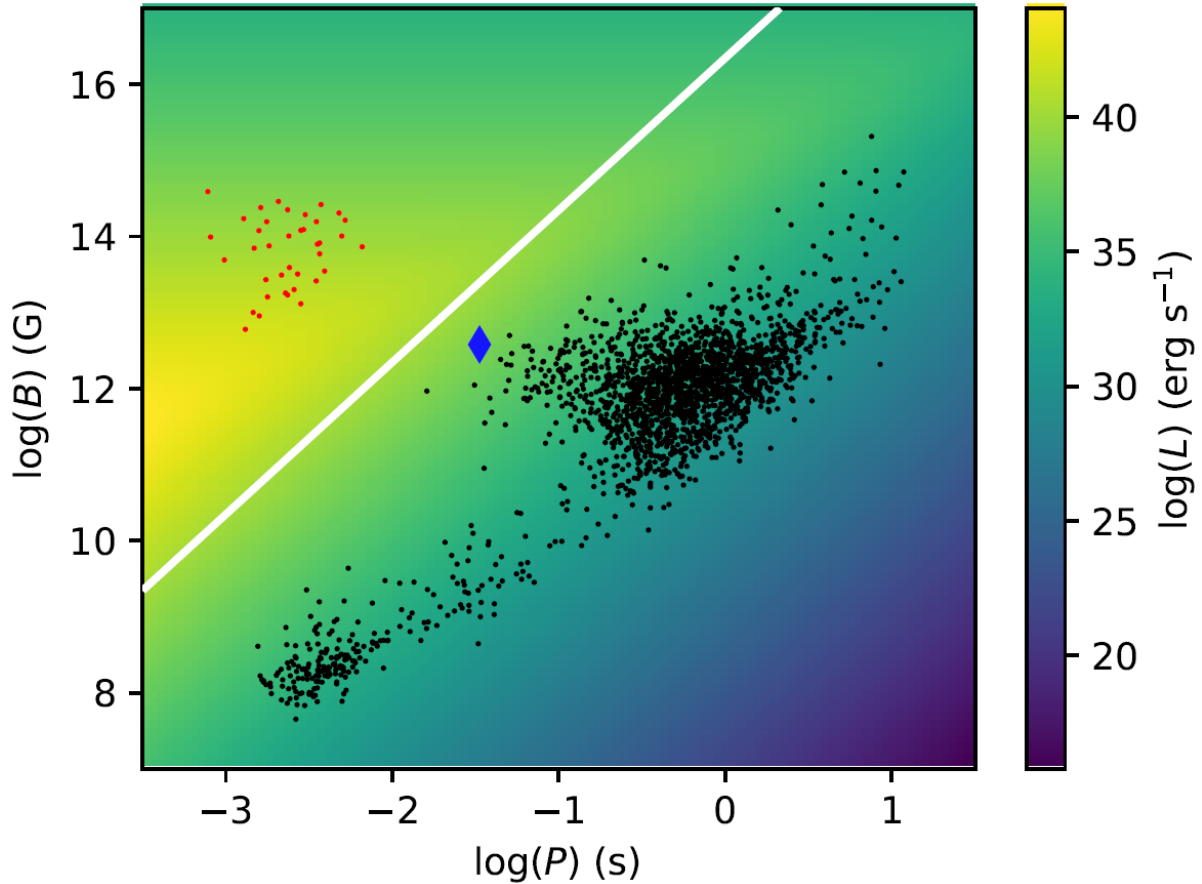


**Figure 3.3:** Galactic pulsars (black) and pulsar parameters inferred from extragalactic SLSNe (red), distributed in the  $BP$ -plane. The galactic pulsars are shown at their current parameters. Their initial parameters must have been located to the left. The extragalactic pulsars in the centre of SLSNe are plotted at their initial periods. The straight line indicates a constraint on  $B$  and  $P$ , at given pulsar luminosity  $L$  in SN 2002ap at the time of observation in 2018. The blue diamond corresponds to the pulsar in the Crab nebula, as reference.

strength  $B$ , means that their rotation period change is high and they are moving fast to the right in the  $BP$ -plane.

Now we aim to analyse the magnetic field strength  $B$  (which we assume to be constant over time) and the initial period  $P_0$  right after the core collapse. From this data we can then model the time-dependent behaviour of the central compact object as described in equation (2.4).

In order to find  $B$ , we take the magnetar’s characteristic age into account, as in-

roduced in equation (2.4). Plotting the maximum allowed initial luminosity, we find a curved line whose horizontal left part then gives us the magnetic field limit of the magnetar, as presented in Figure 3.4. We see that the luminosity decreases above the curved line for higher magnetic fields. It is therefore a lower limit on the magnetic field,  $B \gtrsim 10^{13.5}$  G.

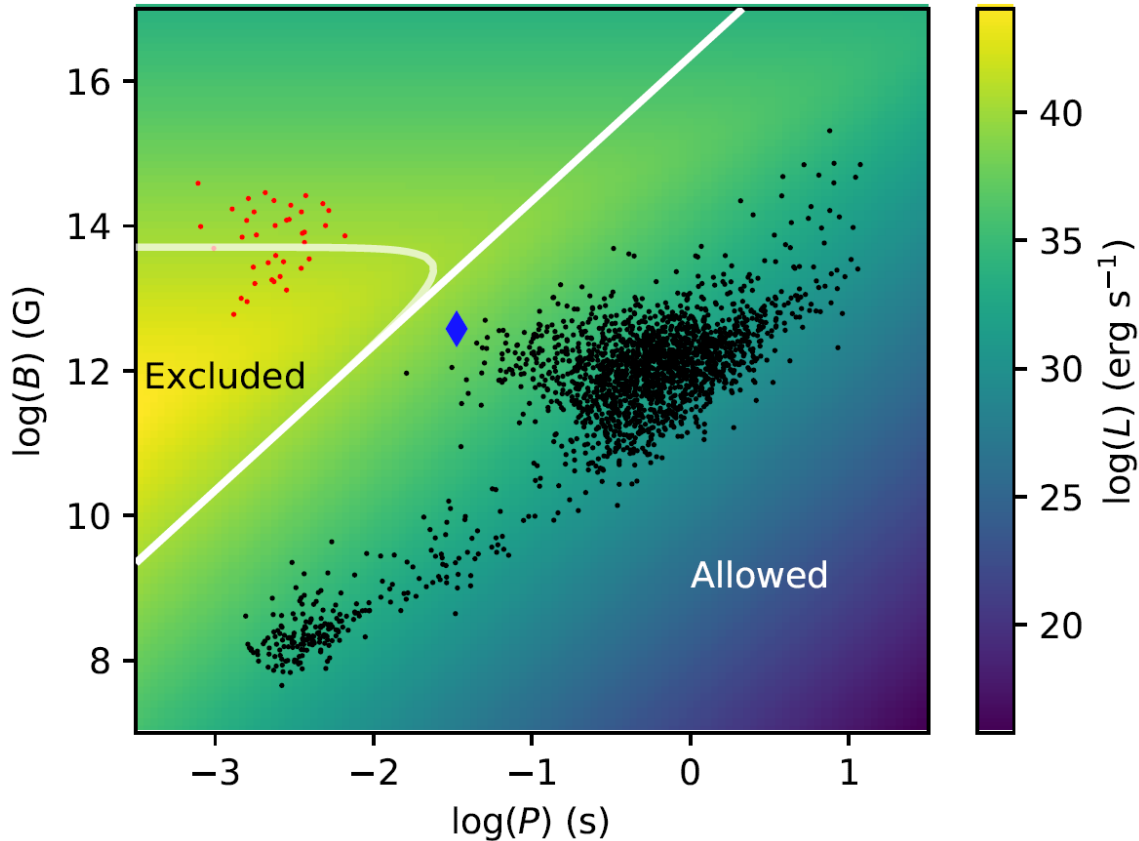


**Figure 3.4:** Same as Figure 3.3, with the constraint on the initial luminosity (curved line) of SN 2002ap added, in addition to the current luminosity in 2018 (straight line).

We denote an area excluded since we have an upper limit on the luminosity, and the type Ic-BL implies an initial period  $P_0 < 0.01$  s. Since the luminosity is greater within the region labelled “Excluded” than in the region above, we conclude that the magnetar in the centre of SN 2002ap might never have been located in that region.

The rotation period of neutron stars, whose magnetic field is assumed to be constant, increases as they lose rotational energy. Thus, the magnetar studied here also moves to the right hand side of the  $BP$ -plane. As we have found an upper limit of the luminosity,

we expect the SN to have passed the straight line at the time of observation with Chandra. Thus, we denote this area as allowed.

### 3.5.3 Compiling results

Studying Figure 3.4 we see that there is a straight line and a curved line part of the  $BP$ -plane. The straight line corresponds to the parameter constraints at the time of the Chandra measurement. That is, the line, corresponding to the maximal allowed luminosity, provides an upper limit for the parameter  $B$  and a lower limit for the period  $P$  at the time of observation. The curved line, in turn, comes from the time dependency as mentioned in equation (2.4) and corresponds to the initial luminosity. We note that the magnetic field is constant along the first part of the curved line. Since we have an upper limit on the luminosity, this horizontal part constitutes a lower limit on the magnetic field  $B \gtrsim 10^{13.5}$  G. From the total energy required to produce a Ic-BL SN, we can also expect an initial period time to be in the same range as the SLSNe depicted as red data points.

In Chapter 3.3, we argued what the maximal luminosity is allowed to be if we assume to have a magnetar in the centre, since we only measured one incoming photon in the source region. The luminosity limit we have calculated is of order  $10^{40}$  erg s<sup>-1</sup>. This result and the constraint on the magnetic field imply that the central object of SN 2002ap is probably a magnetar. We see furthermore that it may be similar to the central engines in those SLSNe that have high magnetic fields, i.e. the red points above the magnetic field limit in the  $BP$ -plane, as seen in Figure 3.4.

# Chapter 4

## Discussion

### 4.1 Initial rotation period

In order to understand why a supernova can become so luminous we wish to study its energy sources. According to the magnetar model there is a neutron star in the centre. Its rotation, we suppose, supplies the energy manifesting in the luminosity we measure. However, the rotation is slowing down with time as the neutron star loses energy. To gain information about the early phases of the SN we aim to find the initial parameters. With this information we can draw further conclusions on the whole SN evolution, including time periods before that the ejecta becomes transparent for photons.

In Figure 3.3, the straight line is the limit of the luminosity at the time of measurement, as given by the magnetic field strength  $B$  and rotational period  $P$ . Given the time since the initial explosion we assume SN 2002ap nowadays shall appear in the right hand side of the  $BP$ -plane, underneath this line. The magnetic field of the neutron star is assumed to be constant and the rotational period will increase as the spinning object slows down. To visualise this in the model, imagine a newly emerged neutron star showing up as a data point in the  $BP$ -plane. As time passes, the point drifts to the right hand side of the figure. Initially this process is swift, but with time it gets progressively slower. The relationship describing the change in period time with regard to the current period of a neutron star makes this apparent. Rewriting equation (3.5) we find the relation

$$\dot{P} = \frac{8\pi^2 R^6 (B \sin \alpha)^2}{3c^3 I} \cdot \frac{1}{P}, \quad (4.1)$$

where  $c$  is the speed of light,  $\dot{P}$  is the change in rotational period,  $R$  is the radius of the star,  $I$  is the moment of inertia and  $\alpha$  is the angle between the rotational- and magnetic axes (Condon and Ransom 2016). Following this equation,  $\dot{P}$  becomes smaller as  $P$  increases. We can interpret it as follows: the increase of the period time becomes slower but remains positive for all times.

Thus, we can assume that the red SLSNe points in Figure 3.4 do drift to the right hand side as well. Eventually a quasi-stationary state is reached as  $P \rightarrow \infty$ .

We can also study SN 2002ap at other energy intervals. Wang et al. (2017) have used data in the UVOIR spectrum to estimate the initial parameters. They have found the magnetic field strength  $B = 1 \cdot 10^{16}$  G, and the initial period  $P_0 = 20$  ms. For comparison, we can use equation (2.5) to estimate some initial rotation periods by trying out different values for the magnetic field strength. We present our initial period values in Table 4.1 and plot these values and Wang’s result in Figure 4.1.

**Table 4.1:** Initial period  $P_0$  of the pulsar in the centre of SN 2002ap for different values along the straight line, corresponding to current periods at the time of observation.

$\log(B)$ [G]	$P(t)$ [s]	$P_0$ [ms]
14	0.100	1.67
15	0.316	5.29
16	1.000	16.7

In the figure, we see that the difference between the logarithms of the current period and the initial period is independent from the magnetic field strength. Although the magnetic field strength in Wang et al. (2017) is high, their numerically obtained initial period value is close to the value we get analytically for a similarly high magnetic field strength. However, the value of the initial period is highly dependent on the assumptions on the current period and the magnetic field strength, as  $P(t)$  and  $B$  are also unknown in equation (2.5). The initial periods we find are just based on speculations on the constraints on  $P(t)$  and  $B$ , as the current values are estimates of the parameters at the time of observation in 2018.

Mazzali et al. (2002), who also have studied the UVOIR spectrum of SN 2002ap, have found that it must have been on the mass frontier between black holes and neutron stars, possibly being a black hole. If that is the case, the conclusion regarding the mass frontier seems to be consistent with the mass parameter results of Wang et al. (2017). However, Wang et al. (2017) have concluded that the compact object of SN 2002ap should be a magnetar instead of a black hole.

Logically, we should expect to find data points for different SNe in the entirety of the  $BP$ -plane and not just clusters in sporadic parts of it, as seen in Figure 3.4. It is always important to remember that the models astrophysicist use aim to compare similar groups of SNe, as well as approximations of their magnetic fields and initial rotation periods. Furthermore, clusters of closer objects are generally easier to observe. Since they often have similar, cluster-specific features, they might deviate from the average, influencing

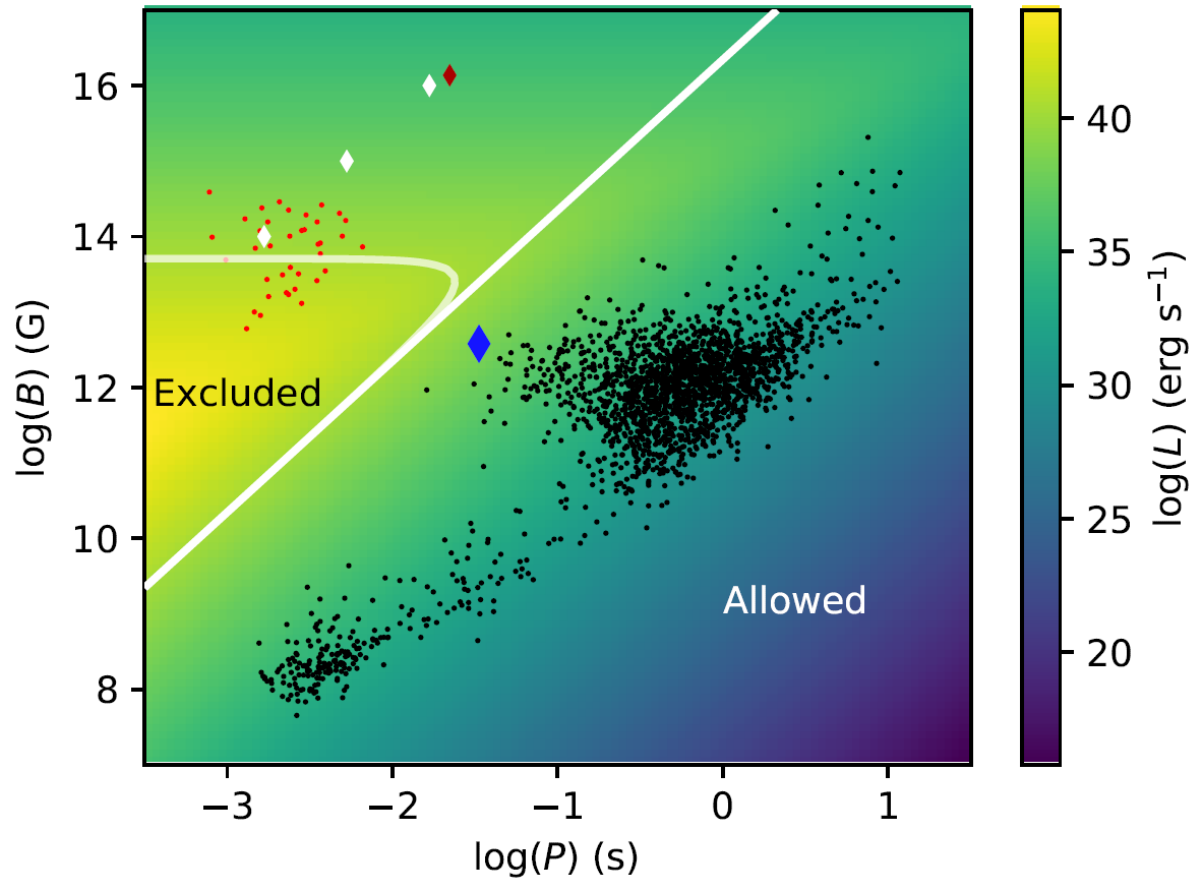


**Figure 4.1:** Pulsars in the centre of SNe and SLSNe, distributed in the  $BP$ -plane. Same as Figure 3.4, with our estimated initial periods from Table 4.1 (white diamonds) and Wang’s initial period results (red diamond) added.

our theories. Nevertheless, data points should presumably appear in between as well, which we might discover in the future as technology develops.

## 4.2 Limitations and future observations

The main sources of uncertainties in the model are the chosen parameters for the absorption. The area of research for this thesis is still highly theoretical and new findings are regularly reported. That said, our parameters for elemental abundances are based around the reference values of a common CCSN, and we have made rough estimations when applying them to the Ic-BL type SN 2002ap.

The models we use are highly simplified ones. In order for us to be able to construct deeper constraints, we should start our observations earlier or make them at a closer position to the SN. The latter is possible by observing a closer SN, if one appears. However, SN 2002ap has been observed since the point that its progenitor star exploded and is one of the closest SNe discovered. The main problem is that the ejecta are generally too dense in the first years for the photons to traverse them. Consequently, if we cannot register any incoming photons – since they are absorbed before reaching our detector – we can only speculate about the processes going on during the first years after the explosion. At later times when the ejecta has become transparent, the rotation has abated so much that the neutron star has ceased to emit significant amounts of energy.

Our study is based on the X-ray interval 2 – 10 keV and we assume that 1.6 % of the energy of the central compact object of SN 2002ap is emitted in this range. The satellite measurement we have used was made in 2018, when the ejecta had already expanded enough for the X-ray radiation to get through it. Despite this, the telescope registered only one photon in the source region during 16 ks, which is consistent with most ordinary galactic neutron stars that have rotation periods on the order of 1 s. Thus, we can explain the lack of registered photons in our observation by the presumption that the rotation frequency of the neutron star has become too low. Furthermore, we shall keep in mind that our model is purely theoretical, since we have not had enough data from the studied SN to fit it to.

Ultimately, more data, new models and more precise and efficient telescopes are needed to further our understanding of SNe and the driving forces behind them.

# Chapter 5

## Summary and conclusions

To summarise, we used X-ray telescope data to find an upper limit for the luminosity of the central object of SN 2002ap. We derived this limit by assuming that this object is a neutron star with a strong magnetic field, a magnetar. Also, we aimed to find the corresponding magnetic field strength limit of the magnetar. Handling the data from the Chandra telescope with numerical absorption modelling, we found the maximal flux of this magnetar. Then, we obtained its total bolometric luminosity using the distance of the object and an assumption on how much of the total radiated energy was included in the observed energy interval. Next, we used this luminosity value to find a lower limit on the magnetic field that the magnetar in SN 2002ap might have.

We found that the maximal bolometric luminosity is on the order of  $10^{40}$  erg s<sup>-1</sup>, 16 years after the explosion. This coincided well with the luminosity based on the visible light wavelengths. Thus, we concluded that the magnetar could have contributed to the high luminosity of SN 2002ap.

Furthermore, we found that the minimal magnetic field of the magnetar is approximately  $10^{13.5}$  G. Comparing this value to the estimations made by Nicholl et al. (2017) for other, similar SNe, we could conclude that our magnetic field limit is high, but since the estimates of Nicholl et al. (2017) were mainly within one order around our result, it should still be a plausible estimate.

To find an exact initial rotation period and deeper constraints is of further interest. We have seen that in order to obtain these, we need to make observations at an earlier time in the development, or perhaps observe a closer SN with a more sensitive telescope. However, these come up against the difficulty that the ejecta absorbs most of the high energy radiation. Furthermore, we wish to find objects in the whole  $BP$ -plane. There should reasonably be data points that we have not discovered yet in the empty areas in Figure 3.4. More data and new telescopes may provide the solution in the future.

# Bibliography

- Alp, Dennis et al. (2018). ‘X-Ray Absorption in Young Core-collapse Supernova Remnants.’ In: *The Astrophysical Journal* 864.2, p. 175. DOI: <https://doi.org/10.3847/1538-4357/aad737>.
- Arnaud, Keith et al. (2020). *Xspec users’s manual: Introduction*. URL: <https://heasarc.gsfc.nasa.gov/xanadu/xspec/manual/node2.html>. (accessed: 22.03.2021).
- Astrophysics, Harvard-Smithsonian Center for (2002). *Location of SN 2002ap before and after the explosion in M74*. URL: <https://lweb.cfa.harvard.edu/supernova/images/sn2002ap.gif>. (accessed: 21.04.2021).
- (2012). *Chandra Hardware*. URL: <https://chandra.harvard.edu/about/hardware.html>. (accessed: 22.03.2021).
- (2013). *Telescope system*. URL: [https://chandra.harvard.edu/about/telescope\\_system.html](https://chandra.harvard.edu/about/telescope_system.html). (accessed: 22.03.2021).
- Astrophysics, Harvard-Smithsonian Center for (2014). *The Chandra Mission*. URL: [https://chandra.harvard.edu/about/axaf\\_mission.html](https://chandra.harvard.edu/about/axaf_mission.html). (accessed: 26.02.2021).
- Berkowitz, Joseph (1979). *Photoabsorption, Photoionization, and Photoelectron Spectroscopy*. Academic Press. ISBN: 9780323148283.
- Condon, James J. and Scott M. Ransom (2016). *Essential Radio Astronomy*. Princeton, New Jersey: Princeton University Press.
- Fermilab, Today (2013). *Cross section*. URL: [https://www.fnal.gov/pub/today/archive/archive\\_2013/today13-03-01.html](https://www.fnal.gov/pub/today/archive/archive_2013/today13-03-01.html). (accessed: 21.05.2021).
- Gelderman, Dr. Richard (2012). *Hubble’s Distance - Redshift Relation*. URL: [http://astro.wku.edu/astr106/Hubble\\_intro.html](http://astro.wku.edu/astr106/Hubble_intro.html). (accessed: 02.03.2021).
- Hondongwa, Donald B. and Eric R. Fossum (2014). ‘A Review of the Pinned Photodiode for CCD and CMOS Image Sensors’. In: *IEEE Journal of the Electron Devices Society* 2, pp. 33–43. DOI: <https://doi.org/10.1109/JEDS.2014.2306412>.
- Janka, H.-Th. et al. (2007). ‘Theory of core-collapse supernovae’. In: *Physics Reports* 442, pp. 38–74. DOI: <https://doi.org/10.1016/j.physrep.2007.02.002>.
- Karttunen, H. et al. (2007). *Fundamental Astronomy*. Springer. ISBN: 9783540341437.
- Manchester, R.N. et al. (2005). ‘The Australia Telescope National Facility pulsar catalogue.’ In: *The Astrophysical Journal* 129. DOI: <https://doi.org/10.1086/428488>.

- Mazzali, P.A. et al. (2002). ‘The Type Ic Hypernova SN 2002ap’. In: *The Astrophysical Journal* 572, pp. L61–L65. DOI: <https://doi.org/10.1086/341504>.
- Metzger, Brian D. et al. (2014). ‘Ionization break-out from millisecond pulsar wind nebulae: an X-ray probe of the origin of superluminous supernovae.’ In: *Monthly Notices of the Royal Astronomical Society* 437, pp. 703–720. DOI: <https://doi.org/10.1093/mnras/stt1922>.
- NASA/CXC (2019). *Illustration of Chandra Spacecraft Components*. URL: <https://chandra.harvard.edu/about/spacecraft.html>. (accessed: 23.03.2021).
- NASA/CXC/S. Lee (2009). *Illustration of Chandra Spacecraft Components*. URL: <https://chandra.harvard.edu/resources/illustrations/teleSchem.html>. (accessed: 14.05.2021).
- Nicholl, Matt et al. (2017). ‘The Magnetar Model for Type I Superluminous Supernovae. I. Bayesian Analysis of the Full Multicolor Light-curve Sample with MOSFiT.’ In: *The Astrophysical Journal* 850. DOI: <https://doi.org/10.3847/1538-4357/aa9334>.
- Smale, Dr. Alan (2018). *X-ray Telescopes - More Information*. URL: [https://imagine.gsfc.nasa.gov/observatories/technology/xray\\_telescopes2.html](https://imagine.gsfc.nasa.gov/observatories/technology/xray_telescopes2.html). (accessed: 19.03.2021).
- Taddia, F. et al. (2019). ‘Analysis of broad-lined Type Ic supernovae from the (intermediate) Palomar Transient Factory’. In: *Astronomy & Astrophysics* 621, A71. DOI: <https://doi.org/10.1051/0004-6361/201834429>.
- Wang, L.J. et al. (2017). ‘Evidence for Magnetar Formation in Broad-lined Type Ic Supernovae 1998bw and 2002ap’. In: *The Astrophysical Journal* 837, p. 128. DOI: <https://doi.org/10.3847/1538-4357/aa5ff5>.
- Willingale, R. et al. (2013). ‘Calibration of X-ray absorption in our Galaxy’. In: *Monthly Notices of the Royal Astronomical Society* 431 issue 1, pp. 394–404. DOI: <https://doi.org/10.1093/mnras/stt175>.
- Wilms, J. et al. (2000). ‘On the Absorption Of X-Rays in the Interstellar Medium’. In: *The American Astronomical Society* 542, pp. 914–924. DOI: <https://doi.org/10.1086/317016>.

